Blister-based-laser-induced-forward-transfer: A non-contact, dry laser-based transfer method for nanomaterials

Blister-Based-Laser-Induced-Forward-Transfer: A Non-Contact, Dry Laser-Based Transfer Method for Nanomaterials

N.T. Goodfriend[1,2], S.Y.Heng[1], O.A. Nerushev[1], A.V. Gromov[1], A.V. Bulgakov[2,3], M. Okada[4], R. Kitaura[4], J. Warner[5], H. Shinohara[4], E.E.B. Campbell[1,6,*]

1. EastCHEM, School of Chemistry, University of Edinburgh, David Brewster Road, Edinburgh EH9 3FJ, Scotland.

2. HiLASE Centre, Institute of Physics of the Czech Academy of Science, Za Radnici 828, 25241 Dolní Břežany, Czech Republic

3. S.S. Kutateladze Institute of Thermophysics SB RAS, 1 Lavrentyev Ave., 630090 Novosibirsk, Russia

4: Department of Chemistry, Nagoya University, Nagoya 464-8602, Japan

5: Department of Materials, University of Oxford, 16 Parks Road, Oxford OX1 3PH, U.K.

6: Division of Quantum Phases and Devices, School of Physics, Konkuk University, Seoul 05029, Korea

Abstract

We show that blister-based-laser-induced forward transfer (BB-LIFT) can be used to cleanly desorb and transfer nano- and micro-scale particles between substrates without exposing the particles to the laser radiation or to any chemical treatment that could damage the intrinsic electronic and optical properties of the materials. The technique uses laser pulses to induce the rapid formation of a blister on a thin metal layer deposited on glass via ablation at the metal/glass interface. Femtosecond laser pulses are advantageous for forming beams of molecules or small nanoparticles with well-defined velocity and narrow angular distributions. Both fs and ns laser pulses can be used to cleanly transfer larger nanoparticles including relatively fragile monolayer 2D transition metal dichalcogenide crystals and for direct transfer of nanoparticles from chemical vapour deposition (CVD) growth substrates, although the mechanisms for inducing blister formation are different.

I. INTRODUCTION

The clean transfer of nanomaterials such as monolayer graphene or 2D transition metal dichalcogenides (TMDC) onto target substrates is crucial for the fabrication of nanodevices that will exploit the excellent electrical or optical properties of the pristine nanomaterials. Conventional transfer techniques typically involve the use of thermal release tape[1,2] or a sacrificial PMMA (polymethylmethacrylate) film[3] to support the nanomaterials during etching of the growth substrate. However, it is extremely difficult to completely remove all residual traces from the transfer medium, resulting in the degradation of the intrinsic properties of the materials and a reduction of device reliability[4,5]. In recent years many efforts have been made to improve the cleanliness and reliability of the transfer technique[5], however, it is still a major challenge to find a universal technique that does not involve exposing the sensitive nanomaterials to chemical or thermal treatment. In this paper, we demonstrate the application of a technique known as Blister-Based Laser-Induced Forward Transfer (BB-LIFT)[6,7] that allows the transfer of nanostructures without exposing them to any treatment that can introduce impurities and adversely affect their performance.

BB-LIFT is a variation of methods that use laser pulses to transfer material without involving the direct interaction of the laser pulse with the material to be transferred. It is closely related to LIAD (laser-induced acoustic desorption), that is used to introduce thermally labile molecules into the gas phase for spectroscopy or mass spectrometry studies[8] by using a ns laser pulse to back-irradiate a metal foil on which the molecules have been deposited. Although originally attributed to acoustic desorption, the mechanism behind LIAD has been subject to much debate and it is now thought that the desorption mechanism is predominantly thermal in nature[9]. LIFT (laser-induced forward transfer) is a non-contact single-step direct-write technique which employs pulsed laser radiation penetrating a transparent substrate to heat and vaporise a donor film deposited on it[10,11]. BB-LIFT (blister-based laser-induced forward transfer) was introduced for depositing diamond nanoparticles[12] or organic liquid molecules[13] in well-defined microscale patterns on substrates[14]. Instead of a polycrystalline metal foil, a thin metal[12] or polymer[15] layer is deposited on a transparent substrate and the particles or liquid to be transferred are deposited on the thin film. The laser pulse impinges through the transparent substrate to interact with the underside of the metal layer. This interaction induces the formation of a blister on the front side of the film[6,7] that serves to desorb the

material on the front side. There are two mechanisms that have been discussed in the literature to explain the desorption process. One is a thermal mechanism that relies on the different thermal expansion coefficients of the film and the underlying transparent substrate to induce rapid deformation of the film and the other involves laser ablation at the interface between the thin film and the transparent substrate leading to a rapid mechanical deformation of the film material. We have recently shown, by studying the morphology of the thin films after irradiation[6] and the efficiency of gold-coated nanoparticle removal[7], that, when using ns lasers to deform a thin metal film, the mechanism is predominantly thermal in nature with a small mechanical component, whereas fs irradiation leads to a permanent blister deformation of the surface, providing evidence for a mechanical deformation without significant heating of the film or the desorbing particles.

In this paper, we show that the velocity distribution of desorbed particles is very narrow and low when using fs laser pulses for back-irradiation of thin metal films and it can be tuned by changing the thickness of the film. In addition, the angular spread of the desorbed particles is very narrow, providing a well-defined deposition position. We demonstrate the potential of BB-LIFT for cleanly depositing fragile 2D nanomaterials (MoS_2 and $MoSe_2$). We also demonstrate the direct transfer of chemical vapour deposition (CVD) -grown carbon nanotubes from their growth substrate, thus providing a controlled means of depositing nanomaterials without exposing the as-grown materials to any potentially contaminating atmosphere or chemical/thermal treatment.

II. EXPERIMENTAL DETAILS

The transparent substrate (typically a crown glass microscope slide with a thickness of 1mm) was first cleaned by sonication in distilled water with decon to remove any large particles or oil contamination, followed by sonication in methanol and then air plasma treatment. These steps are important to ensure a perfectly clean and defect-free surface prior to the deposition of the metal thin film. This ensures homogeneous adhesion of the metal to the surface and consequently a smooth metal film. For all experiments with the exception of the direct transfer of CVD-grown carbon nanotubes (Section III.D), a thin Ti film was then deposited on the glass microscope slides to a thickness of 200-400 nm using electron beam evaporation under high vacuum conditions. The actual film thickness

was always checked by AFM prior to depositing the nanomaterials. The nanomaterials to be desorbed were deposited on the metal film either from solution using a "sandwich coating" method[7] or spin-coating, or in the case of C_{60} also via oven evaporation. The 2D TMDC crystals were deposited on the metal films either by dropping a dispersed solution on the metal film ($MoSe_2$) or by using a dry PMMA transfer technique (MoS_2)[3]. For BB-LIFT transfer from CVD substrates it was necessary to use a more complex multilayer system with a Ni blister layer in place of Ti, described in section III.D. Multiwalled carbon nanotubes were grown on the substrate using a 1" quartz tube furnace, following the protocol used previously by Nerushev et al.[16]. The quartz tube was flushed with Ar (99.996% purity, 600 sccm) and H_2 (99.96% purity, 100 sccm), at atmospheric pressure. It was then heated to 700˚C and C_2H_2 (technical quality, 8sccm) was introduced for 15 minutes. The C_2H_2 flow was stopped, while the furnace was kept at 700˚C for a further 10 minutes, to flush out excess C_2H_2 and reduce the amount of amorphous carbon deposit. The furnace and quartz tube were then slowly allowed to cool to room temperature before removing the substrate.

The substrates were mounted on an x-y translation stage and irradiated through the transparent substrate under high vacuum conditions (base pressure ca. 3×10^{-7} mbar). Two lasers were used for irradiation; a frequency-doubled (532 nm) Nd:Yag laser with a pulse duration of 7 ns and the fundamental output from a Ti:Sapphire laser at 800 nm with a pulse duration of 120 fs. The fluence conditions for obtaining blister formation were determined previously[6] for Ti films and lie within the range 200-400 $mJcm^{-2}$ and 150 – 300 $mJcm^{-2}$ for ns and fs laser pulses, respectively. Higher fluence values of ca. 600 – 700 $mJcm^{-2}$ were needed for the Ni films (for both ns and fs pulses).

Velocity distributions were determined for both Au-coated silica nanoparticles and for C_{60}. The fullerene was a convenient nanoparticle to determine desorption velocities since many particles (isolated molecules and small crystals) were desorbed from a single blister and the molecules could be easily detected via photoionisation mass spectrometry, providing data with acceptable signal/noise ratios. The comparison with the more massive Au-coated nanoparticles showed that the mechanically-induced velocities were similar in magnitude and determined predominantly by the thickness of the metal layer, related to the velocity of expansion of the blister on the metal film. The desorbed molecules/nanoparticles were allowed to travel for a distance of a few mm before being ionised by a second laser pulse and detected in a simple time-of-flight mass spectrometer.

The delay between the desorbing and the ionising laser pulses was varied and the ion intensity as a function of the delay was recorded. The spectra were averaged for 5-10 individual blisters for each delay.

The angular distributions of the desorbed particles collected on a target substrate were characterised by AFM, optical microscopy and Raman spectroscopy (514 nm).

III. RESULTS AND DISCUSSION

A. Velocity Distributions

Figures 1(a) and (b) show the velocity distributions determined for BB-LIFT of C_{60} films deposited on 200 nm thick Ti films, using ns laser pulses (532 nm) at fluences of 150 ± 45 mJcm^{-2} and 200 ± 50 mJcm^{-2} respectively (note that the uncertainty limits for the fluence values are absolute uncertainties, the relative value is more accurate). The C_{60} film thickness was ca.180 nm. The low fluence value is at the lower limit for ejecting particles and just below the threshold fluence for blister formation[7]. A bimodal distribution is seen for the low fluence that is typical for ns laser desorption of C_{60} films[17]. The data is fitted by a sum of two modified Maxwell-Boltzmann distributions with flow velocities, v_0, superimposed on the thermal distributions, eq. 1.

$$I(v) = A_1 v^2 exp\left(\frac{-m(v-v_{0,1})^2}{2k_B T_1}\right) + A_2 v^2 exp\left(\frac{-m(v-v_{0,2})^2}{2k_B T_2}\right) \quad (1)$$

where A_n adjusts the relative weight of the distributions, m is the molecular mass, v is the velocity, $v_{0,n}$ are the flow velocities, k_B is Boltzmann's constant and T_n are the temperatures.

We interpret the two distributions in terms of the heating of the relatively thick C_{60} layer. The fast component ($T_2 \approx 1500$ K, $v_{0,2} \approx 400$ ms^{-1}) is likely to be from molecules at the interface with the hot metal film that are heated to a temperature similar to that of the hot metal, while the cooler molecules that form the slower component ($T_1 \approx 600$ K, $v_{0,1} \approx 100$ ms^{-1}) are likely to be removed from the upper region of the film via the desorption of the underlying hot molecules. For the higher fluence results in Fig. 2(b) the two thermal distributions have been fitted with $T_1 \approx 700$ K, $v_{0,1} \approx 300$ ms^{-1} and $T_2 \approx 2000$ K, $v_{0,2} \approx 750$ ms^{-1}. An additional non-thermal slow component observed at 200 mJ/cm^2 has been fitted

using a skew normal distribution, eq. (2), with a flow velocity, v_0 (similar to the fits for fs BB-LIFT, discussed below) with a most probable, peak velocity v_p of 106 ms^{-1}.

$$I(v) = Aexp\left[\frac{-(v-v_0)^2}{\sigma}\right]\left(1 + erf\left(\frac{a(v-v_0)}{\sqrt{\sigma}}\right)\right) \quad (2)$$

Where A, σ and a are fit parameters.

The temperatures fitted for the fast, thermal components (1500 K and 2000 K respectively) correlate very well with the expected surface temperature of the metal film, as estimated in a previous publication[6]. The flow velocity is related to collisions in the desorption plume and is expected to be larger for the higher fluence where all molecules are desorbed from the area corresponding to the blister region, leading to an increase in collisions during desorption and a correspondingly higher flow velocity. The slow component observed for the higher fluence C_{60} result is very similar to the velocity distribution measured for much heavier gold-coated silica nanoparticles with diameters of ca. 150 nm at a fluence of 250 ± 50 mJcm^{-2}, Fig. 1(c). In this case it is not possible to observe any thermally-desorbed particles and instead we only detect a slow non-thermal component that is fitted with a skew normal distribution at a peak velocity v_p of 44 ms^{-1}. Velocity distributions determined for C_{60} desorbed using fs laser pulses are shown in Fig. 2. The distributions look very different from the C_{60} distributions measured using ns laser desorption. Only one narrow peak is seen that cannot be fitted with a thermal distribution, similar to the situation shown for the gold-coated silica nanoparticles in Fig. 1(c). The peak has been fitted with a skew normal distribution, eq. (2), in each case. The measured distribution is independent of the value of the laser fluence within the rather limited range that leads to blister formation. This is illustrated in Fig 2(a) where data from 370 nm thick Ti films are shown for fluence values ranging from 250 mJcm^{-2} to 295 mJcm^{-2}. The peak velocity (v_p) is seen to shift to larger velocities and the distribution broadens as the thickness of the metal Ti film is decreased.

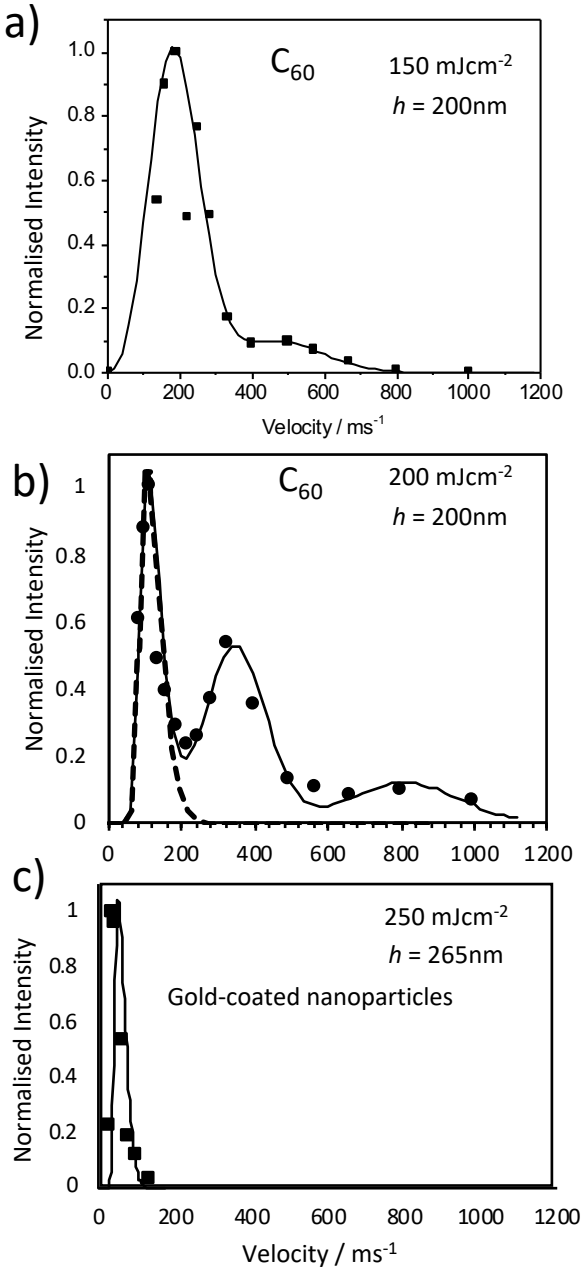

Fig. 1. Velocity distributions of particles removed by ns BB-LIFT (a) C_{60} removed from a 200nm thick Ti film with 150 mJcm^{-2} ns pulses, full line is a fit to the data using two modified Maxwell-Boltzmann distributions (see text for details) (b) as (a) but for 200 mJcm^{-2}, dashed line shows an additional slow, non-thermal component fitted with a skew normal distribution (c) Gold-coated silica nanoparticles removed from a 265 nm thick Ti film with 250 mJcm^{-2} ns pulses, fitted with a skewed normal distribution.

A plot of the peak velocity, v_p, versus the reciprocal Ti film thickness (h) produces a straight-line plot as can be seen in Fig. 3. The peak velocities of the non-thermal components of the ns

BB-LIFT velocity distribution data from Fig. 1, for both the C_{60} and the gold-coated nanoparticles, have been included on this plot. They fit the fs data trend perfectly.

The similar slow velocities observed under fs and relatively high fluence ns LIFT

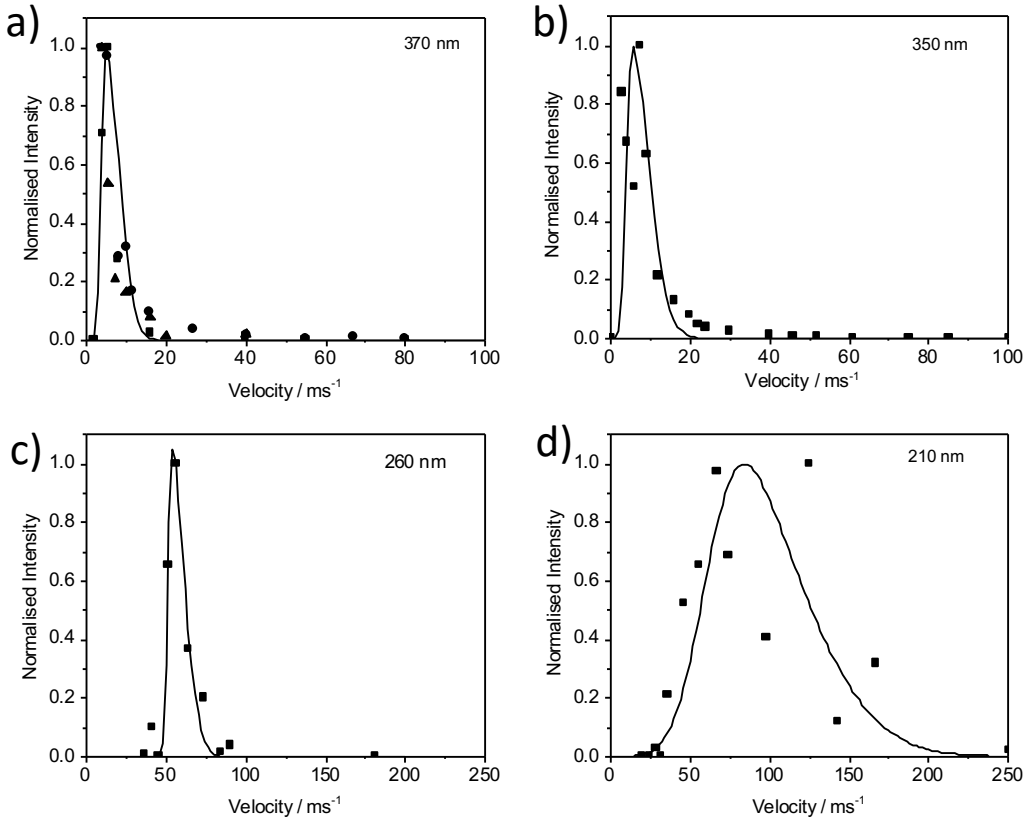

Fig. 2. Velocity distributions of C_{60} removed by fs BB-LIFT (a) 370 nm thick Ti film, circles: 250 mJcm^{-2}, squares: 260 mJcm^{-2}, triangles: 295 mJcm^{-2}. (b) 350 nm thick Ti, (c) 260 nm thick Ti, (d) 210 nm thick Ti. Note the change in velocity scale between (a), (b) and (c), (d)

conditions and the observation that the velocity determined for the much larger gold-coated nanoparticles falls on the same trend line are perhaps rather surprising results. However, they provide strong support for the mechanical nature of the desorption under fs laser conditions and also for the presence of a mechanical component in addition to thermal desorption under ns conditions. The velocity of the mechanically desorbed particles depends predominantly on the thickness of the metal film and hence, presumably, on the velocity of the film deformation.

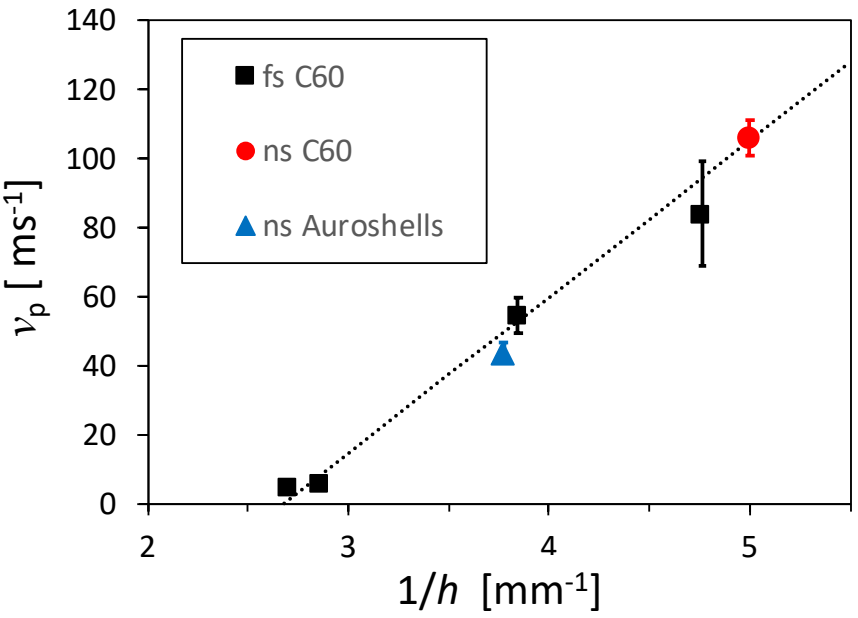

Fig. 3. Velocities, v_p, corresponding to the peak of the velocity distributions for the fs BB-LIFT data from Fig. 2 (black squares) plotted against the reciprocal of the Ti film thickness (h). The velocities corresponding to the peaks of the non-thermal components from ns BB-LIFT for the data plotted in Fig 1(b) and (c) are included for comparison. Red circle: C_{60}; Blue triangle: gold-coated nanoparticles ("Auroshells").

The slow, mechanical component is observed for ns conditions (≥ 200 mJcm^{-2}) that provide thermal stress in the metal film that is comparable to or exceeds the yield stress conditions (ca. 700 MPa for Ti)[7], leading to observable cracking on the film surface. The observation that the gold-coated nanoparticles (diameter ca. 150 nm) sit on the same trend line as C_{60} is very strong support for a mechanical desorption mechanism rather than a thermal desorption. In the case of fs BB-LIFT it can be considered that it is the speed of expansion of the metal film due to the build-up of pressure formed from ablation of the interface region that determines the velocity of the mechanically desorbed particles. A simple consideration of the pressure that is produced on ablation at the interface provides an estimate on the order of 1 GPa, similar to the thermal yield stress value. If one considers the blister deformation under fs conditions to be similar to the deformation of a thin membrane under impulsive pressure loading[18] then one can expect the deformation velocity to scale as the inverse of the film

thickness, as observed here. The offset in the velocity may be associated with the energy needed to remove the nanoparticles from the underlying metal film.

B. Angular Distributions

The angular distributions of the desorbed particles were determined by measuring the spread of particles deposited on a target glass substrate situated 2 – 3 mm in distance from the LIFT substrate. The results are shown in Figs. 4, 5 and 6.

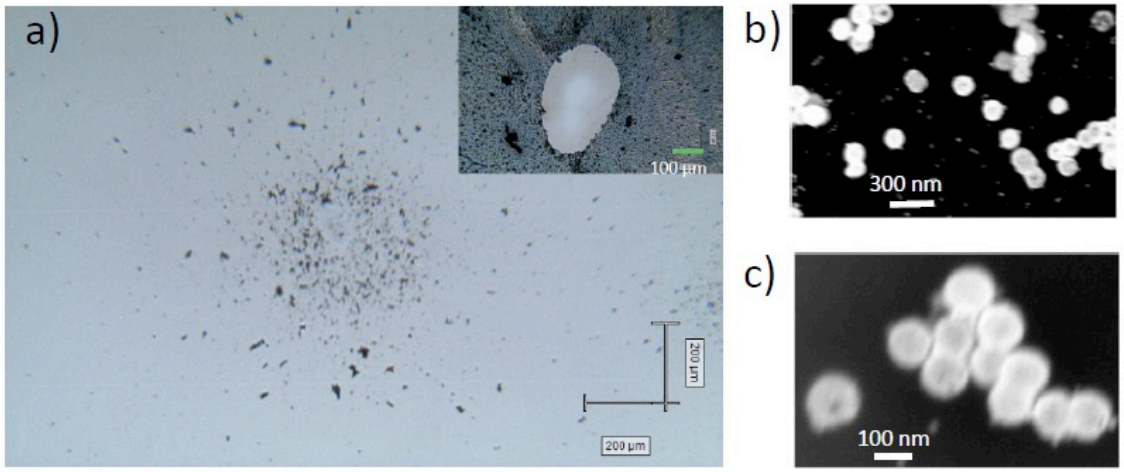

Fig. 4. (a) Spread of gold-coated nanoparticles deposited by ns BB-LIFT at a laser fluence of 250 mJcm^{-2} from a 260 nm thick Ti film. The particles were deposited on a glass substrate situated 2mm away from the donor substrate. Insert: image of a blister post-LIFT showing the removal of all nanoparticles from the central blister region. The scale bars are 200 µm in the main figure and 100 µm for the insert. (b) SEM image of the nanoparticles after deposition on the donor substrate (c) Higher magnification SEM image of nanoparticles after BBLIFT removal and deposition on the glass substrate. No evidence of damage to the nanoparticles can be seem

Figures 4 shows the deposited particles, imaged in an optical microscope and with SEM for ns deposition of gold-coated silica nanoparticles. It can be seen that the nanoparticles are present as agglomerates (larger black patches), both on the donor film (insert) and after deposition. As was discussed in a previous publication[7], the nanoparticles are completely removed from the central, blister region. The SEM images (Fig. 4(b) and (c)) show no evidence of damage to the nanoparticles during the LIFT procedure or when deposited on the target substrate. Although we cannot rule out that the aggregates imaged post-deposition have

been formed after deposition the similarity in density of such aggregates pre- and post-deposition is an indication that the aggregates are transferred and deposited as intact entities.

Optical images of blisters and deposits from fs BB-LIFT deposition of C_{60} are shown in Fig. 5. A very sharp boundary is observed for the deposited particles in Fig. 5(d) but less so for the example in Fig. 5(b). This can be compared to the blister pattern that remains on the donor substrate. The lower fluence/thicker Ti film, Fig. 5(a), shows an intact blister where all fullerenes have been removed from the central region (bright region) with a surrounding ring (magenta) where some but not all of the fullerenes have been desorbed. The fullerene film tends to desorb as small crystallites from the central region, together with isolated molecules, as can be clearly seen from the optical image of deposited particles in Fig. 6. The partial desorption in the outer ring region, leads to a more gradual decrease in the intensity of the deposited particles. For the slightly higher laser fluence/thinner Ti film, Fig. 5(c), there is some clearly visible distortion or damage in the centre of the blister and a sharper definition of the blister boundary. Within this boundary all fullerene particles are removed from the

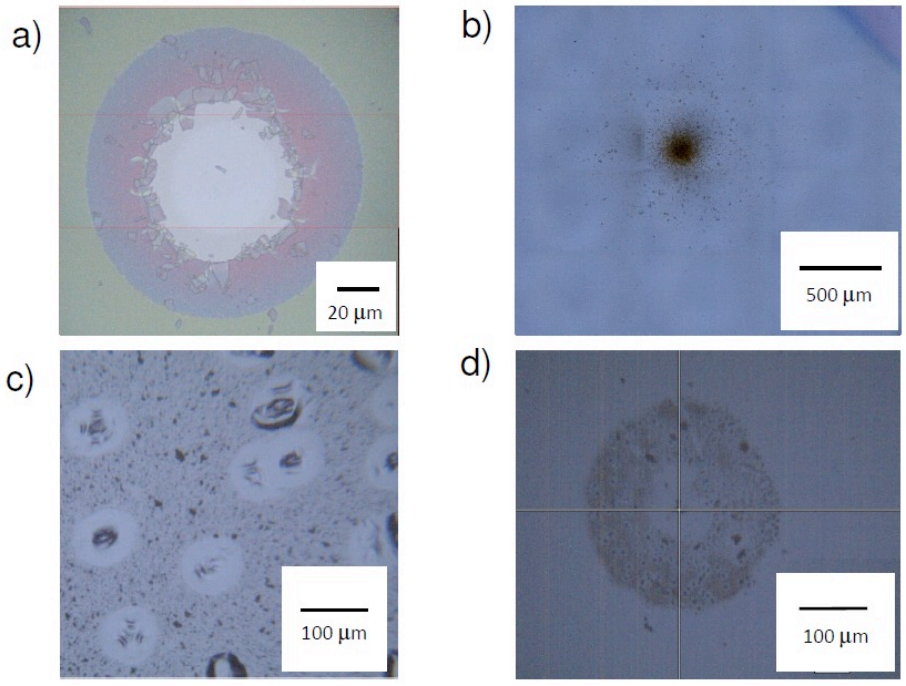

Fig. 5. Optical microscope images of fs BB-LIFT deposited C_{60} and the blisters formed on the donor substrate. (a) Blister formed on a 310 nm thick Ti film coated with ca. 180 nm C_{60}, laser fluence 180 mJcm^{-2}. The light central region is the raised Ti film (blister) with no fullerenes remaining, the surrounding lilac ring has a residual coating of fullerenes (but thinner than the original film, outer region). (b) Deposit built up from desorption from 50 blisters obtained under the desorption conditions in (a). Donor-target distance 2mm (c) Blisters formed on a 220 nm thick Ti film spin-coated with C_{60}, laser fluence 200 mJcm-2. (d) Deposit built up from desorption from 50 blisters obtained under the desorption conditions in (c). Donor target distance 3 mm.

substrate but outside the boundary, the particles deposited on the Ti film appear to be unaffected. The distortion in the centre of the blisters is also reflected in the lower intensity of deposit in the central region, Fig. 5(d), indicating some deflection either during desorption or on impact. The thinner Ti film leads to a higher peak velocity (Fig. 3) that may also lead to some scattering or break-up of crystals on impact. Similar to the situation with the gold-coated nanoparticles, for the C_{60} deposition it appears that the small fullerene crystallites on the donor substrate are largely transferred intact to the target surface (Fig. 6). Raman spectra before and after deposition show no evidence of degradation of the material with the characteristic $A_g(2)$ C_{60} mode appearing at the same wavenumber (1469 cm^{-1}) in each case.

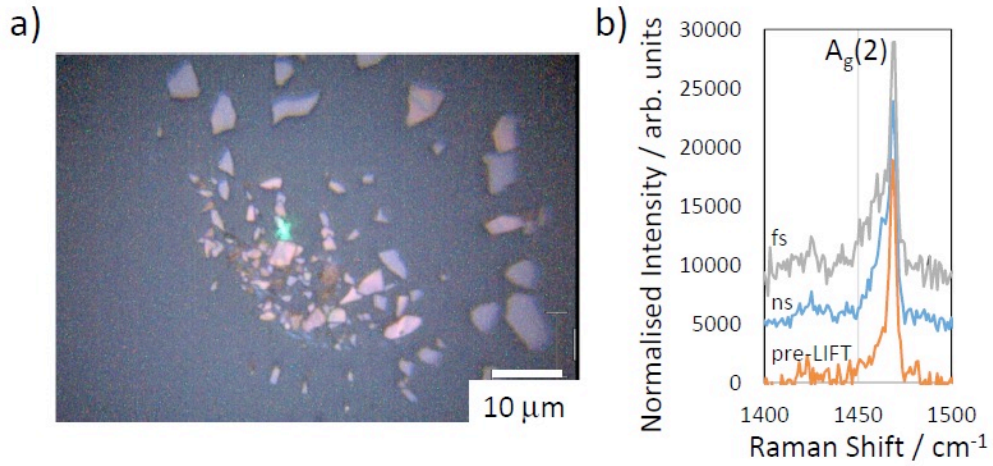

Fig. 6. (a) High resolution optical microscope image of fullerene crystallites that have been deposited intact on a target substrate. (b) Raman spectra (514nm) of fullerene material prior to BB-LIFT (lowest spectrum), ns BB-LIFT deposited material (middle spectrum) and fs BB-LIFT deposited material (top spectrum). The position of the characteristic $A_g(2)$ peak is identical in each case.

The results of the analysis of the optical microscope images of the deposits are summarised in Fig. 7. The deposit from ns laser BB-LIFT C_{60} shows the largest radial spread. The extent of the spreading is consistent with the high desorption temperature obtained from the fits of the velocity distributions (Fig. 1). Although the gold-coated nanoparticles have been desorbed under similar conditions the radial distribution is better defined and indicates a spread of only ca. 5° from the substrate normal, consistent with the lack of a thermal velocity component for these much larger particles. The pattern of the gold-coated nanoparticle deposit formed from intact blisters is similar to that of the fs laser BB-LIFT desorbed C_{60} shown on Fig. 7 (c). The red lines in Fig. 7 are $\cos^n\theta$ distributions with $n = 200$ (Fig. 7(b)) and $n = 580$ (Fig. 7(c)) to demonstrate the very highly directed nature of the deposition. The data is also consistent with a relatively flat region that corresponds approximately to the radius of the blister on the donor

substrate followed by a decrease in intensity scaling as 1/Radius, as illustrated in Fig. 8. As was shown previously, the blisters obtained with ns irradiation have a larger diameter than those formed with fs radiation for similar laser spot dimensions[6]. This is a consequence of the fs laser blister corresponding to the area within the laser pulse where the energy is sufficient to cause ablation of the underside of the metal film.

The deposition from the fs BB-LIFT of C_{60} on the thinner Ti film, Fig. 7(d), is less homogeneous. There is an inner region of the deposit that has an anomalously low intensity of deposited particles. A similar, but less pronounced, minimum is also visible in the gold-coated nanoparticle data that has been obtained from burst blisters, shown as the grey data points in Fig. 7(b). The inhomogeneous deposition in the central area thus seems to be associated with inhomogeneity or disruption of the blister which becomes more pronounced for thinner Ti films. The higher impact velocity from the thinner Ti film, v_p = 77 ms^{-1}

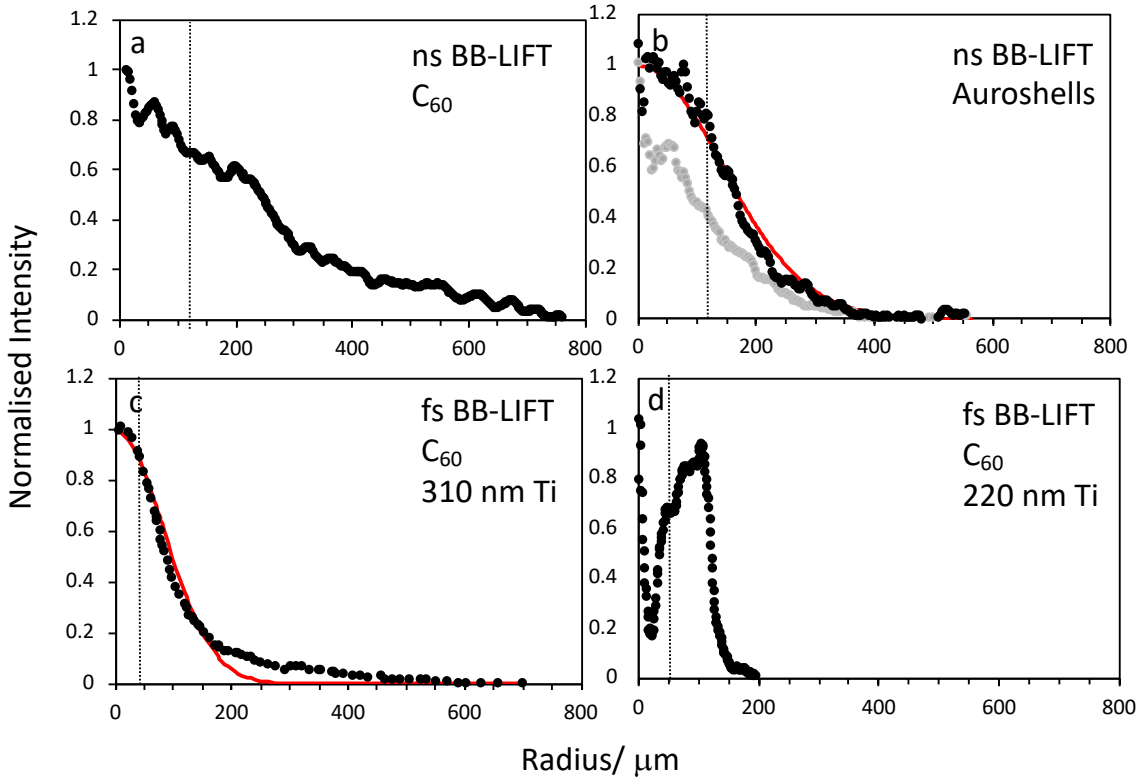

Fig. 7. Normalised radial distributions of deposited particles. The origin of the x-axis is at the centre of the deposited material. (a) ns BB-LIFT, 250 $mJcm^{-2}$, C_{60}, sum of 200 blister deposits, donor-target distance 2.8 mm (b) ns BB-LIFT, 250 $mJcm^{-2}$, gold-coated nanoparticles, black: sum of 30 deposits from intact blisters, grey: sum of 10 deposits from burst blisters, donor-target distance 2 mm. Red line: $\cos^{200}\theta$ distribution. (c) fs BB-LIFT, 180 $mJcm^{-2}$, C_{60}, sum of 50 deposits, donor-target distance 2 mm. Red line: $\cos^{580}\theta$ distribution. (d) fs laser BB-LIFT, 200 $mJcm^{-2}$, sum of 50 deposits, donor-target distance 3 mm. The vertical dashed lines indicate the radii of the blisters on the donor substrate in each case.

compared with v_p= 27 ms^{-1} for the thicker film (Fig. 3) could also lead to scattering or destruction of crystallites on impact although the very sharp boundary region visible in Figs. 5(d) and 7(d) does not support this interpretation.

C. Transfer of 2D transition metal dichalcogenide crystals

The results discussed in the previous sections indicate that the velocity of particles desorbed using fs BB-LIFT is low and largely determined by the thickness of the Ti film. The intact transfer of fullerene crystallites (Fig. 6) indicated that it may be possible to transfer fragile and considerably larger 2D transition metal dichalcogenide crystals. This could provide a convenient means for fabricating nanodevices, particularly on transparent substrates.

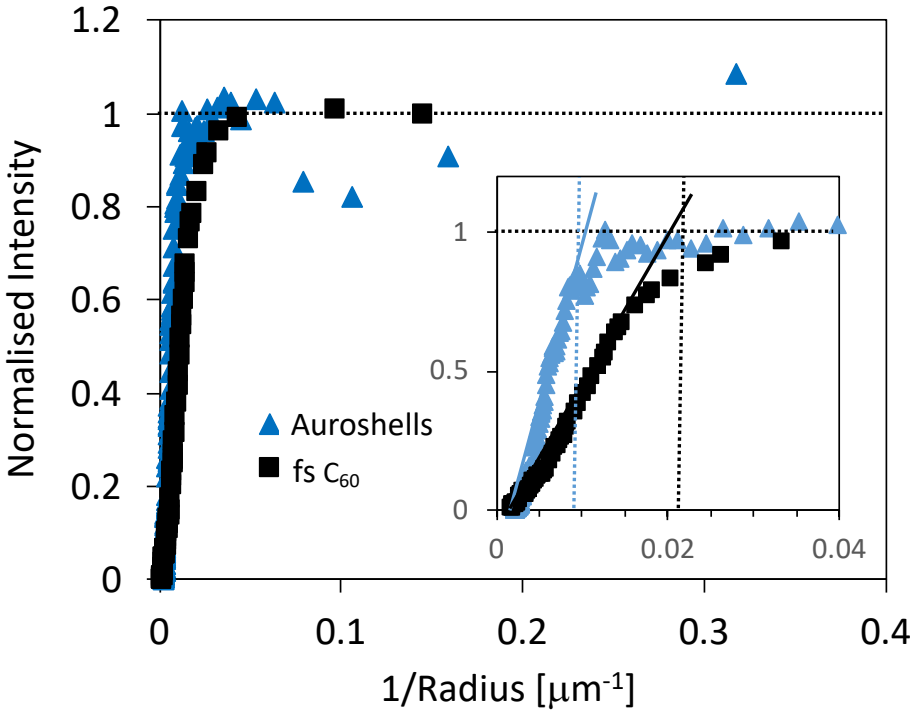

Fig. 8. Data from Fig. 7(b) (blue triangles, gold-coated nanoparticles) and Fig. 7(c) (black squares, C_{60}) plotted as a function of the inverse deposition radius. The inset shows the data close to the origin. The vertical dashed lines indicate the radii of the BB-LIFT blisters.

$MoSe_2$ crystals were grown by CVD and deposited on a BB-LIFT substrate (300 nm thick Ti) by dropping a suspension of the material onto the metal film and allowing it to dry. A sparse deposition of crystals of a variety of sizes was produced on the Ti as can be seen in Fig. 9(a). Raman spectra of the individual crystals showed that they were predominantly multilayers. Fig. 9(b) shows a ca. 30µm x 20 µm crystal that has been successfully transferred by fs BB-LIFT to a silicon chip. The Raman spectra before and after transfer with a peak position at

242 cm^{-1} shown in Fig. 9(c) indicate that the crystal had more than 4 layers[19]. The inset shows the same crystal prior to being transferred. For successful transfer the laser has to impact the BB-LIFT substrate directly below the crystal to be transferred. When this occurs the transfer success rate is 100%. On a few attempts the particle was "hit" off-centre which appeared to lead to fragmentation or rotation of the crystal during flight.

Monolayer crystals of MoS_2 were grown by CVD[19] and deposited on a BB-LIFT substrate (250 nm thick Ti) using a dry transfer method[3]. This provided a sample with a higher density of more homogeneous crystals, Fig. 10 (a). The figure also shows a number of blisters. Each blister completely removes and transfers any crystals that were on its surface. The higher

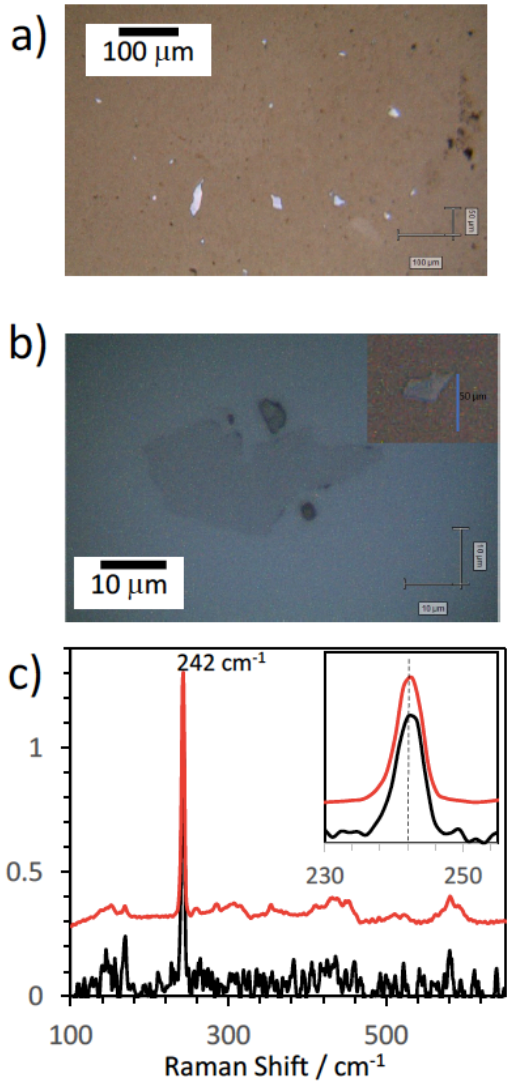

Fig. 9. (a) Optical microscope image of dispersed $MoSe_2$ crystals deposited on a BB-LIFT substrate (250nm thick Ti). (b) Optical microscope image of a crystal transferred to a Si chip. Insert: the same crystal prior to transfer. (c) Normalised Raman spectra of the crystal before (red, upper) and after (black, lower) transfer. The position of the peak at 242 cm^{-1} indicates that the crystal has > 4 layers.

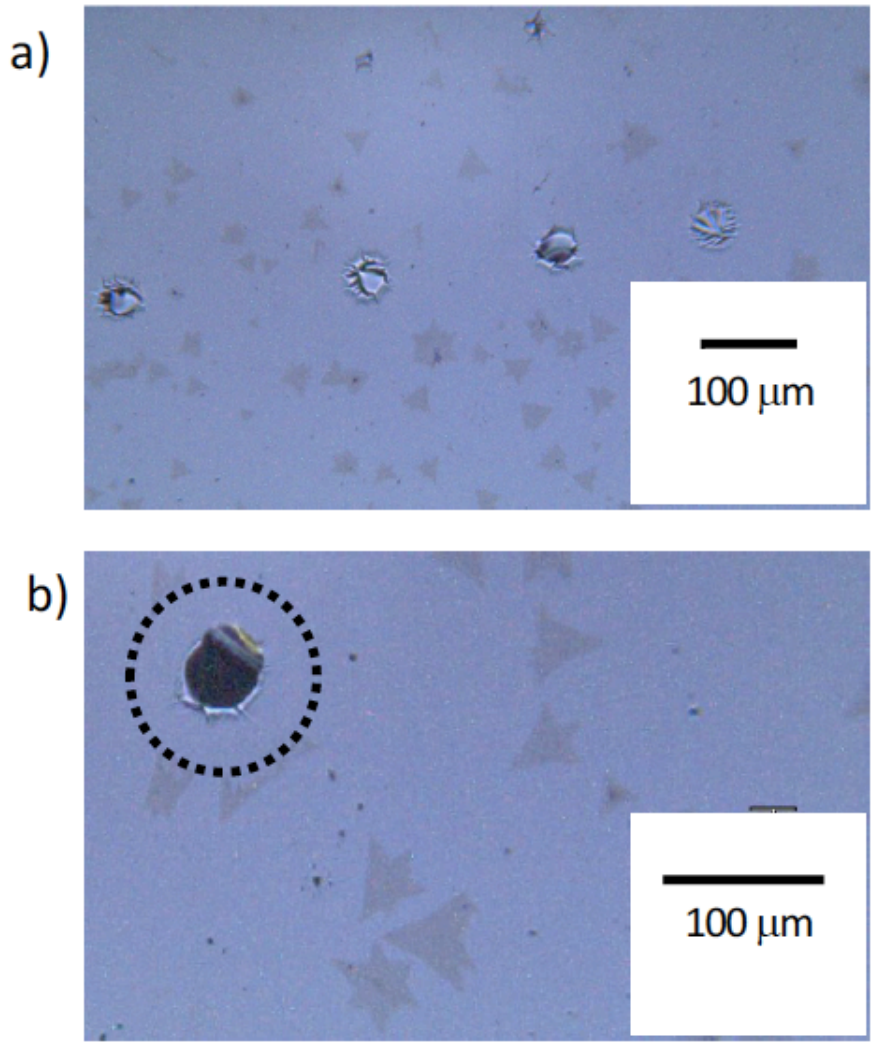

Fig. 10. Optical microscope images of MoS_2 crystals deposited via a dry transfer method on to a BB-LIFT substrate (250 nm thick Ti). (a) Blisters produced by fs laser pulses are visible, the central region of the blister in each case has partially collapsed and shows up clearly in the image. (b) A higher magnification image showing one blister that has burst in the centre. The blister diameter is larger than the burst region and is indicated but the black circle. No MoS_2 crystals remain within the total blister region.

magnification image in Fig. 10(b) shows a blister that has burst in the centre but at the edges of the blister it is clear that crystals on the surface have been cleanly broken at the blister edge. This was not observed for the thicker multilayer $MoSe_2$ crystals. The AFM image in Fig. 11 (a) shows one of these transferred crystals where the edges have been cleanly cut by the boundaries of the blister. The Raman spectra in Fig. 11 (b) show E_{2g} and A_{1g} peak

positions that are consistent with a monolayer crystal[21] and also that there is no change in the Raman spectrum before and after transfer.

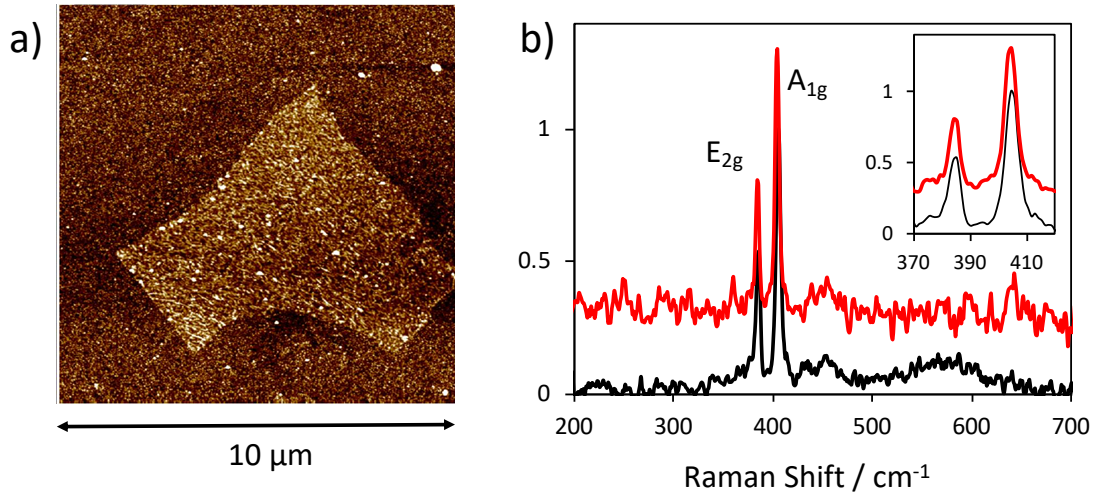

Fig. 11. (a) AFM image of a transferred MoS_2 crystal. (b) Normalised Raman spectra before (red, upper) and after (black, lower) transfer. The peak positions indicate that the transferred crystal is a monolayer.

D. Transfer of CVD-grown carbon nanotubes

In the previous section it was demonstrated that fs BB-LIFT could be used to transfer fragile monolayer TMDC crystals from one substrate to another. However, the main benefit of this technique would be to avoid any mechanical or chemical processing of the materials after growth while fabricating devices from the materials. In section III.C the crystals first had to be deposited on a BB-LIFT compatible substrate either by dropping a dispersion or using a dry transfer method. The ideal application of the BB-LIFT transfer technique for functional nanomaterials would be to remove materials from substrates on which they have been grown using e.g. chemical vapour deposition and, without exposing the grown materials to any chemical treatment, cleanly deposit them in a controlled fashion on a substrate for device fabrication. So far, no substrate that has been demonstrated for CVD growth of high quality

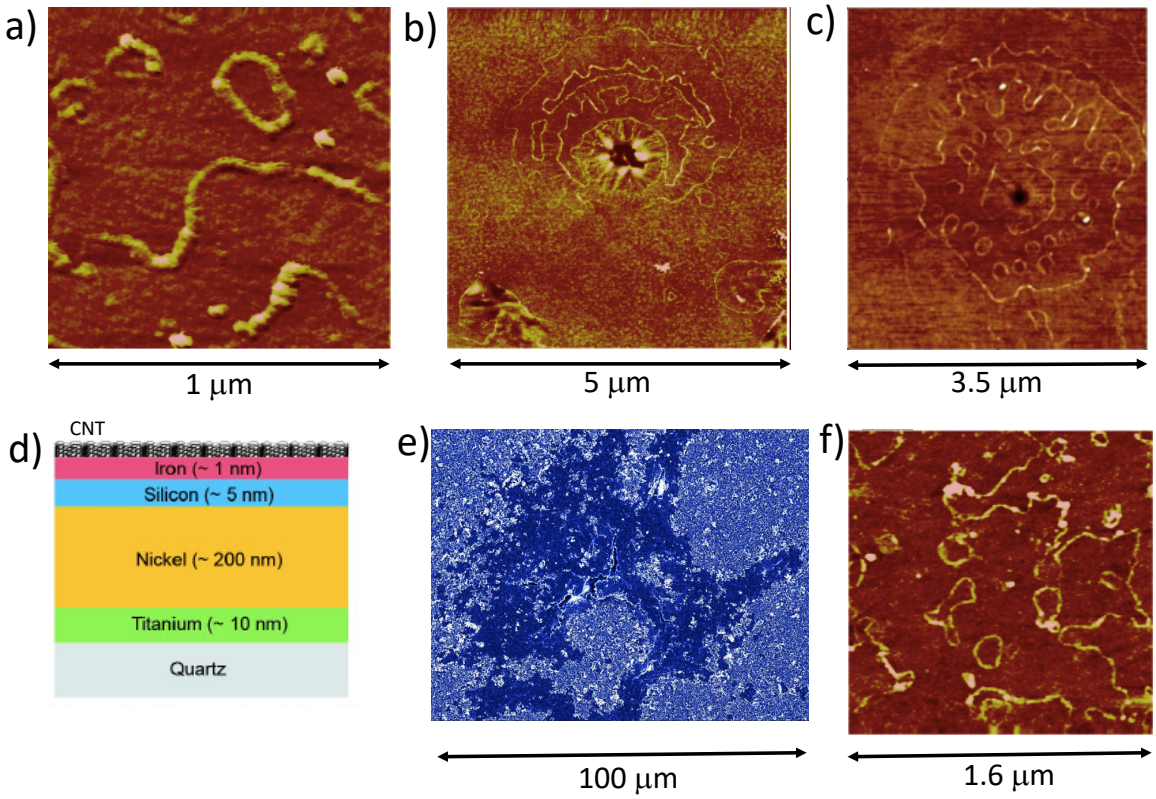

Fig. 12. (a) AFM image of spin-coated multi-walled nanotubes transferred to a silicon chip using fs BB-LIFT with a 200nm thick Ni film. (b) AFM image of spin-coated single-walled nanotube bundle transferred to a silicon chip using fs BB-LIFT. (c) As (b) but for ns BB-LIFT. (d) Schematic of the layered substrate used to both grow carbon nanotubes using CVD and to directly transfer the grown nanotubes using both fs and ns BB-LIFT. (e) Scanning electron microscope image of a blister region on the donor substrate, obtained using a fs laser pulse. (f) AFM image of thin multi-walled carbon nanotubes transferred from the CVD growth substrate using fs BB-LIFT.

2D TMDC crystals is compatible with the BB-LIFT method (ability to survive the high temperatures and corrosive atmospheres), although it is conceivable that this could be developed. Instead, a BB-LIFT substrate was modified to be compatible with the CVD growth of multi-walled carbon nanotubes in order to demonstrate the potential of the method for clean transfer from growth substrates. The substrate used for growth and subsequent BB-LIFT is shown schematically in Fig. 12(d). Fused silica was used as the transparent base, in order to withstand the growth temperature of 700 ^{o}C, followed by a 10 nm thick layer of Ti, a 200 nm thick layer of Ni, a 5 nm thick layer of Si or Al and finally a 1 nm thick layer of Fe as CVD growth catalyst. The Ni layer functions as the BB-LIFT layer. Ti could not be used for the BB-LIFT layer in this case since it reacted with the underlying silica under the CVD

growth conditions to form titanium silicide and became translucent. It was, however, found to be necessary to include the 10 nm Ti as an adhesive layer when depositing Ni.

The transfer of commercial multi-walled (ca. 10 nm diameter) and single-walled (ca. 1.0 ± 0.4 nm) nanotubes that were deposited by spin-coating a dispersion of nanotubes on a conventional BB-LIFT substrate but using 10 nm Ti (as an adhesion layer) and 200nm Ni instead of a thin Ti film was first studied. It was determined that blisters could be formed by both fs and ns laser pulses at fluences of ca. 600 $mJcm^{-2}$ in both cases. Fig. 12(a) shows an AFM image of the multi-walled nanotubes transferred to a silicon chip when using a fs laser to form the blister. The presence of a surfactant coating around the nanotubes can be seen in the AFM image. The results of the transfer were similar for blisters produced by both fs and ns lasers. This was also the case for the removal of gold-coated nanoparticles where the mechanism for removing the particles is predominantly mechanical in nature even when using ns laser pulses. Similarly, spin-coated single-walled nanotube samples could be transferred using both fs and ns laser-induced blisters. The single-walled nanotube dispersions contained some small nanotube bundles of around 3-4 nm diameter[22]. Interestingly, when these single-walled nanotube samples were transferred it was occasionally possible to observe unusual structures on the target surface that may have been caused by the bundles breaking up on impact. Figures 12(b) and (c) show AFM images of such structures obtained using fs, Fig. 12(b), and ns, Fig. 12(c), BB-LIFT. The structures characteristically had a small hole in the centre with a diameter of ca. 5 nm and a depth of at least 5nm and were surrounded by individual single-walled nanotubes, either as long "wavy" tubes surrounding the central hole or as small rings.

The nanotubes that were grown on the multilayer BB-LIFT substrate (Fig. 12(d)) were small, relatively sparse, defect-rich multi-walled nanotubes (no efforts were made to optimise the growth conditions for the complex substrate) with a Raman D/G peak ratio of 0.9 ± 0.1 and a diameter of ca. 3 nm. The laser conditions for producing blisters were the same as for the Ti/Ni substrates used to desorb the spin-coated nanotube samples. The transfer of nanotubes without any contaminants from the underlying substrate layers was successful, Fig. 12(f). As for the spin-coated materials, transfer was possible with both fs and ns laser-induced blisters. Figure 12(e) shows an electron microscope image of a blister formed on the donor substrate by a fs laser pulse. The central, darker region is the Si/Fe layer on which the nanotubes were grown. This shows some cracking in the central region due to the expansion of the underlying Ni layer. Nanotubes have been removed from this darker region. The surrounding lighter

region is the original CNT film. The blister is less homogeneous than those produced on the less complex Ti/Ni film used to desorb the spin-coated nanotubes where they appeared as clearly defined circular regions on the surface, similar to those shown for the Ti films in Fig. 10. The observed inhomogeneity is not unexpected considering the complexity of the multilayer substrate and can be largely attributed to inhomogeneity in the thickness of the deposited layers. The small multi-walled nanotubes have been cleanly transferred to the target silicon chip, Fig. 12(f). Raman spectra of the transferred nanotubes were consistent with the spectra of the films with a D/G ratio of 0.8 ± 0.1.

IV. CONCLUSIONS

We have shown that BB-LIFT using thin metal layers can be used to controllably desorb molecules, small crystals and nanomaterials, including 2D TMDC crystals and carbon nanotubes, from substrates without the laser pulse impinging on the material to be desorbed. The blister-formation mechanisms are different when using ns laser pulse durations and fs laser pulse durations. The thermal nature of the ns BB-LIFT mechanism was confirmed by studying the velocity distributions of fullerene molecules. For conditions in which the blister remains intact on the surface, the bimodal velocity distributions can be fitted by two Maxwell-Boltzmann distributions at high temperatures (>1000 K) modified by stream velocities. A non-thermal component was observed in the mass spectra of post-ionised molecules under conditions where thermal stress introduced cracks on the blister surface of the BB-LIFT substrate. BB-LIFT using fs laser pulses shows no evidence for any thermal contribution in the velocity distributions. The velocity of the desorbed particles is low (compared to the thermal velocities) and has a very narrow distribution. The most probable velocity of the desorbed particles scales with the inverse thickness of the metal film and covers the range of a few ms^{-1} to ca. 100 ms^{-1}. The angular distributions confirm the difference in desorption mechanisms with much more directed deposition of fullerenes using fs laser pulses than for ns pulses. For larger nanoparticles such as gold-coated nanoparticles, 2D crystals or nanotubes, it was not possible to observe any thermal desorption from the BB-LIFT substrate using ns laser pulses. In this case, although the metal film is being heated to a temperature on the order of 2000 K, the particles are being mechanically desorbed at relatively low velocities and in a direction very close to the surface normal. No thermal damage to any of the particles was observed.

All of the nanomaterials that have been investigated here, 1nm diameter C_{60}, 150 nm diameter gold-coated silica spheres, ca.1-5 μm long SWNT and MWNT and ca. 30μm x 20μm TMDC crystals, can be transferred by BB-LIFT. The transfer is possible using either ns laser pulses or fs laser pulses as long as the laser conditions are such that a blister is produced in the metal film. It is the rapid formation of the blister – whether due to the build-up of pressure as a consequence of laser ablation at the interface between the transparent substrate and the metal film (fs), or due to thermal stress as a consequence of rapid heating of the metal (ns)– that is responsible for the non-thermal slow velocity component observed for fullerene desorption and for all "massive" nanoparticles. In all cases the thin metal film is rapidly deformed leading to a low temperature impulsive removal of particles with a velocity that simply scales with the thickness of the metal film. In the case of ns laser pulses there is a rapid heating of the metal film and that can be seen to lead to thermal desorption of fullerenes, in addition to the impulsive component that has a low translational temperature. There is no evidence of a thermal component for the fullerenes that are removed using fs laser pulses. For larger nanoparticles, 2D-TMDC or carbon nanotubes, the particles are too large with too strong an interaction with the metal substrate to be easily removed thermally, however the impulsive component is still present (for both ns and fs laser pulses) and allows the particles to be transferred at low velocity and with negligibly small angular deflections, irrespective of the laser pulse duration, as long as a blister is formed in the thin metal film.

In order to desorb large thermally labile molecules for transfer between substrates or for studies in the gas phase, it is preferable to use fs laser pulses where there is no heating of the surface of the metal film and the molecules are desorbed at ambient temperature with a low and well-defined velocity that can be controlled by varying the thickness of the metal layer. Relatively high densities can be achieved by desorbing thick molecular layers. The potential disadvantage is that any crystals or agglomerates of the molecules on the BB-LIFT substrate will also be desorbed largely intact. For practical molecular beam sources of isolated molecules it may be necessary to introduce an additional controlled heating step to break up aggregates followed, if necessary, by gas cooling.

The potential usefulness of this simple technique for fabrication of nanodevices was demonstrated by showing the clean desorption and transfer to a silicon chip of fragile monolayer 2D TMDC crystals using fs laser pulses. Finally, the transfer of carbon nanotubes from a modified BB-LIFT substrate on which the nanotubes were grown using CVD was demonstrated with both fs and ns laser pulses. This opens up the possibility for directly

transferring CVD-grown nanomaterials to substrates for device fabrication without exposing the sensitive nanomaterials to any impurities that may affect their intrinsic electronic and optical properties.

V. ACKNOWLEDGEMENTS

E.E.B. Campbell acknowledges a JSPS Invitation Fellowship with hospitality from the University of Nagoya and the EPSRC Doctoral Training Partnership Fund for partial support of N.T. Goodfriend. N.T. Goodfriend and A.V. Bulgakov acknowledge financial support from the European Regional Development Fund and the state budget of the Czech Republic (project BIATRI: CZ.02.1.01/0.0/0.0/15_003/0000445) and from the Ministry of Education, Youth and Sports (Programs NPU I-project no. LO1602).

To comply with RCUK requirements, the raw experimental data used in the paper can be found at http://dx.doi.org/10.7488/ds/2364

.

VI. REFERENCES

1. T.L. Chen, D.S. Ghosh, M. Marchena, J. Osmond, V. Pruneri, ACS Appl. Mater. Interfaces **7,** 5938 (2015).
2. J. Song, *et al.* Nat. Nanotechnol. **8,** 356 (2013).
3. Y. Sheng, *et al.* Nanoscale **8,** 2639 (2016).
4. Y. Chen, X.L. Gong, J.G. Gai, Adv. Sci. **3,** 1500343 (2016).
5. Z. Zhang, *et al.* Nat. Commun. **8,** 14560 (2017).
6. N.T. Goodfriend, *et al*. Appl. Phys. A **122,** 154 (2016).
7. A.V. Bulgakov, *et al.* J. Opt. Soc. Am. B **31,** C15 (2014).
8. U. Sezer, *et al. Anal. Chem.* **87**, 5614 (2015).
9. F. Calegari, *et al.* J. Phys. B At. Mol. Opt. Phys. **49**, 142001 (2016).
10. M. Colina, M. Duocastella, J.M. Fernández-Pradas, P. Serra, J.L. Morenza, J. Appl. Phys. **99,** 84909 (2006).
11. C. Boutopoulos, A.P. Alloncle, I. Zergioti, P. Delaporte, *Appl. Surf. Sci.* **278,** 71 (2013).
12. T.V. Kononenko, P. Alloncle, V.I Konov, M. Sentis, Appl. Phys. A **94,** 531 (2008).
13. N.T. Kattamis, M.S. Brown, C.B. Arnold, J. Mater. Res. **26,** 2438 (2011).
14. M.S. Brown, C.F. Brasz, Y. Ventikos, C.B. Arnold, J. Fluid Mech. **709,** 341 (2012).
15. M.S. Brown, N.T. Kattamis, C.B. Arnold, Microfluid. Nanofluidics **11,** 199 (2011).
16. O.A. Nerushev, M. Sveningsson, L.K.L. Falk, F. Rohmund, J. Mater. Chem. **11,** 1122 (2001).
17. B. Winter, R. Mitzner, Ch. Kusch, E.E.B. Campbell, I.V. Hertel, J. Chem. Phys. **104**, 9179 (1996).
18. K. Micallef, A.S. Fallah, D.J. Pope, L.A. Louca, Int. J. Mech. Sci. **65**, 177 (2012).
19. P. Tonndorf *et al*., Optics Exp. **21**, 4908 (2013).
20. S. Wang *et al.,* Chem. Mater. **26**,6371 (2014).

21. H. Li *et al*., Adv. Funct. Mater., **22**, 1385 (2012).

22. P. Angelikopoulos *et al*., J. Phys. Chem. C **114**, 2 (2010).